Skin Effect

Lainey Ward

4 March, 2021

Abstract

Using mutual induction, the phenomenon of skin effect is examined by varying current frequency in a double solenoid-conductor unit. A significant correlation is found between voltage and frequency from which the radius of the inner solenoid and the conductor skin depth are calculated. It is determined that copper has the greatest skin depth for a given frequency, followed by aluminium and brass. Their corresponding conductivities are calculated to be (68.9±9.2), (50.8±6.6), and (27.5±3.5) MS/m. The experimental findings coincide to a moderate degree with that of theory.

1 Introduction

The phenomenon of skin effect occurs when alternating current distributes throughout a conductor such that the current density is confined to a region close to the conductor surface. It is a function of permeability, electrical conductivity and current frequency. The effect arises from the interaction of induced eddy currents. [1]

2 Theory

2.1 Induction

There are two distinct types of electric fields; those attributed directly to electric charges, and those associated with changing magnetic fields. The latter is described by Faraday's laws of induction which predicts that a spatially varying electric field induces a time-varying magnetic field, and vice versa.

Taking a loop of wire at rest, the Biot-Savart law reveals that the current through the loop is proportional to the produced magnetic field. [2]

Applying the Biot-Savart law to a solenoid, a coil of many loops, the magnetic field is shown to be:

$$B_0 = \mu H \tag{1}$$

with μ, the magnetic permeability of the solenoid, and H, the magnetic field strength where:

$$H = \frac{N_1 I_1}{L_1} \tag{2}$$

with N_1, the number of turns, I_0, the current, and L_1, the length of the solenoid.

The magnetic flux through each turn is:

$$\Phi_1 = B_0 A_1 = \frac{N_1 I_1}{L_1} \mu \pi R^2 \tag{3}$$

with A_1, the cross-sectional area of the solenoid.

Note that throughout Section 2 the relative permeability of the solenoid (μ_r) is unaccounted for. The relative permeability of non-ferromagnetic metals is approximately 1 and so it is adequate to assume $\mu_0 \approx \mu_0 \mu_r$ for brass, aluminium and copper. [3]

2.2 Mutual Induction

For two loops of wire at rest, the magnetic flux through the second loop (Φ_2) is also proportional to the current through the first loop. This constant of proportionality (M) is known as the mutual inductance of the two loops. Using the reciprocity theorem, it can be shown that the value of M is the same regardless of whether the current runs through the first or second loop. Thus mutual inductance is expressed where:

$$M = \frac{N_2 \Phi_{21}}{I_1} = \frac{N_1 \Phi_{12}}{I_2} \tag{4}$$

The equality of mutual inductance is exploited in the experimental configuration shown in Fig. 1 where alternating current flows through the outer solenoid, creating a spatially varying electric field. Through induction, magnetic flux arises in the outer solenoid and through mutual induction magnetic flux and current also arise in the inner solenoid. [1]

A metal may become magnetically saturated when an increase in the applied current cannot induce magnetism any further. [4] This phenomenon is further discussed in Section 4.

2.3 Eddy Currents

According to the universal flux rule, varying magnetic flux induces an electric field known as counter-electromotive force (back emf). The induced back-emf

in the inner solenoid due to the outer solenoid is:

$$\epsilon_2 = -M\frac{dI_1}{dt} \tag{5}$$

Furthermore, when such an emf occurs in close proximity to a conductive material, closed loops of current form in planes perpendicular to the magnetic field, around the magnetic field lines. Such loops are known as eddy currents. According to Lenz's law, eddy currents tend to flow in such a direction that the flux it produces tends to cancel the change in current. [1].

In this way, the varying magnetic flux within the inner solenoid in Fig. 2 induces eddy currents within the conductive rod.

2.4 Skin Effect

The skin effect occurs due to the interaction of the induced electric current and the opposing eddy currents. Eddy current density tends to be highest at the centre of a conductor and so current in this region is strongly counteracted, and reinforced at the circumference. Thus the current is force to the surface of the conductor, reducing its effective area. [4]

The skin depth (δ) is the distance from a conductor's surface at which the current density falls by a factor of $1 - 1/e$ (≈ 63 %). Skin depth can be described where: [1] [5]

$$\delta = \sqrt{\frac{1}{\pi\sigma\mu_0 f}} \tag{6}$$

with σ, electrical conductivity and f, current frequency.

It is apparent that current frequency is inversely proportional to skin depth. Therefore, at sufficiently high frequencies, the skin depth is less than the thickness of the conductor rod (R_r). As the experiment employs the use of high frequencies in the range $(1 - 10)\ kHz$, it is assumed that the skin depth is smaller than the rod radius yet greater than the thickness of air between the rod and inner solenoid. These boundary conditions can be described as follows:

$$R - R_r < \delta < R_r \tag{7}$$

with R, the radius of the inner solenoid.

Furthermore, according to the Wiedemann-Franz law, the electrical conductivity of metals such as copper and aluminium tends to be negatively proportional to temperature. Therefore, it can be inferred that skin depth is positively proportional to temperature. [6] The potential significance temperature in Eq. 6 becomes apparent in Section 4.2.

2.5 Relevant Formulae

In a derivation by Wiederick (1982), the RMS voltage of the inner solenoid (V) can be related to the current frequency where:

$$\frac{V}{f} = \beta\frac{1}{\sqrt{f}} + \alpha \tag{8}$$

with β, the slope, and α, the y-intercept.

Under the conditions given in Eq. 7, Wiederick (1982) also derives a similar relation:

$$\frac{V}{f} = b\delta + \frac{a}{2} \tag{9}$$

where:

$$b = 2\pi^2 N_2 B_0 R_c \tag{10}$$

and

$$a = 2\pi^2 N_2 B_0 (R^2 - R_c^2) \tag{11}$$

Equating the first components of Eq. 8 and 9, rearranging for δ and equating the result to Eq. 6:

$$\sigma = \frac{1}{\pi\mu_0}\sqrt{\frac{b}{\beta}} \tag{12}$$

Similarly, equating the second components gives:

$$a = 2\alpha \tag{13}$$

Substituting α into Eq. 11, and rearranging returns:

$$R = \sqrt{\frac{2\alpha}{2\pi^2 N_2 B_0} + R_c^2} \tag{14}$$

Therefore, a plot of V/f against f^{-2} fit to Eq. 8 can be used to return values for δ, σ and R. Furthermore, these values can be substituted into Eq. 7 to assess the condition's validity.

3 Experiment

3.1 Set-Up

The experiment makes use of a conductor rod of length $(38 \pm 1)\ cm$ with an inner solenoid of (100 ± 5) turns wound around its midsection, as illustrated in Fig. 1. The conductor is inserted into a larger outer solenoid of (1000 ± 25) turns which provides the induction field. The conductor has a rubber stopper end to ensure that the midsections of the outer and inner solenoids align.

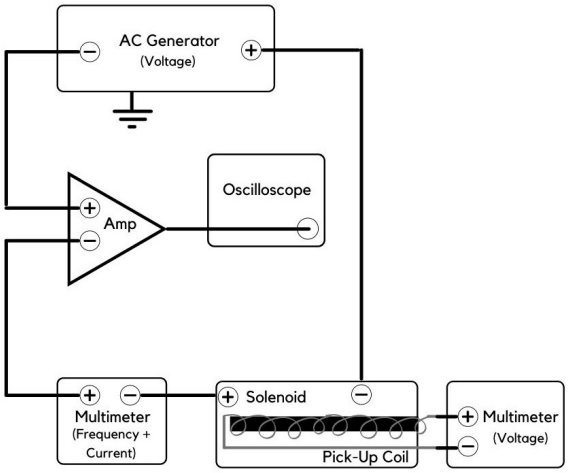

Fig. 1: Circuit diagram of the experimental set-up. The pick-up coil refers to the inner solenoid.

The outer solenoid receives power from a high-frequency AC generator and is connected to a Keysight Model U3606B multimeter. The multimeter displays the primary RMS current (I_{rms}) and the generator frequency, both of which can be adjusted using the frequency and amplitude dials on the AC generator. An amplifier is connected in series to the multimeter and AC generator to increase the gain of the original signal.

The bare ends of the inner solenoid are connected to another multimeter from which secondary RMS voltage (V) is measured.

3.2 Method

A conductor-inner solenoid rod is inserted into the outer solenoid. The frequency is set to approximately 4 kHz and the current to 18 mA. Values for the secondary voltage are recorded over a range of frequency values ($\sim 1-10\ kHz$). The current is readjusted to 18 mA before each reading. Using a calipers, multiple measurements are taken for the radius of the conductor and the inner solenoid. This process repeated for a brass, aluminium and copper conductor rod.

4 Results & Analysis

Unlisted raw data and the propagation of uncertainty are found within the attached Python document.

4.1 Brass Conductor

R_r, R and I_{rms} values are obtained for the brass conductor. Their means are calculated and displayed in Table 1.

Rod	R_r (mm)	R (mm)	I_{rms} (mA)	B_0 (mT)
Brass	4.76±0.02	0.210±0.002	0.220±0.002	0.103±0.004
Aluminium	4.82±0.02	0.210±0.002	0.220±0.002	0.103±0.004
Copper	5.03±0.02	0.210±0.002	0.220±0.002	0.103±0.004

Table 1: Mean values determined for each conducting rod.

The mean I_{rms} is converted to I_1 using Eq. 19. I_1 is substituted into Eq. 1 from which B_0 is found to be $(0.103 \pm 0.004)\ mT$, as shown in Table 1.

V and f values are also obtained for the brass rod, and given in Table 3. V/f is plotted against f^{-2} in Fig. 2a. Using an Orthogonal Distance Regression (ODR) model, the central portion of the data is fit to Eq. 8 with estimated β and α parameters:

$$\frac{V}{f} = f^{-\frac{1}{2}}(9.26\pm0.12)\times10^{-6}+(3.47\pm0.08)\times10^{-7} \quad (15)$$

The selection method for the range of fitted data is detailed within Section 6.3. In this range, there is a significant strong correlation ($r = .999$ $p < .001$) between V/f and f^{-2}. However, the data model has a moderate coefficient of determination ($r_2 = .72$), indicating that ~ 28 % of the data does not lie along the regression line.

B_0 is substituted into Eq. 10, which returns a value for b of $(0.966 \pm 0.006\times)\ mm\ T$. By substituting β and b into Eq. 12, σ is found to be $(27.5 \pm 3.5)\ MS/m$. This has a percent error of 29.6% relative to that determined under similar conditions by Wiederick (1982).

The y-intercept of Eq. 15 and B_0 are substituted into Eq. 14 from which R' is found to be $(5.10 \pm 0.03)\ mm$. This value for R' is slightly greater than R, as anticipated.

The slope of the theoretical model in Fig. 2a is determined by substituting both the σ_c for brass from Wiederick (1982) and the experimental value for b into Eq. 12. The theoretical value for α cannot be determined and so it is assumed to be equal to its experimental value. Therefore, the purpose of this plot is qualitative rather than quantitative.

Using Eq. 6, the experimental and theoretical δ are determined to lie in the ranges $(0.37 - 1.23)\ mm$ and $(0.41 - 1.35)\ mm$, respectively. The experimental δ values are consistently underestimated with a constant percent error of -8.61%. This is apparent in Fig. 2b, where δ is plotted against f. Using an ODR, the data is fit to Eq. 6 with estimated parameters:

$$\delta = \left(\pi\mu f(2.75 \pm 0.00)10^7\right)^{-\frac{1}{2}} \quad (16)$$

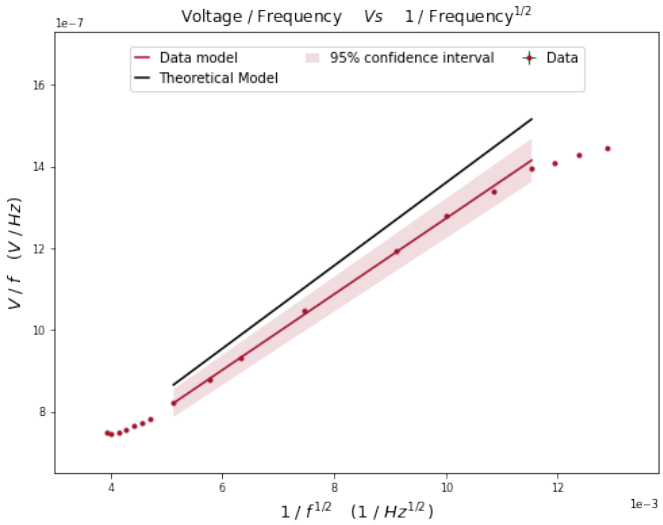

(a) Voltage/frequency plotted against frequency$^{-\frac{1}{2}}$.

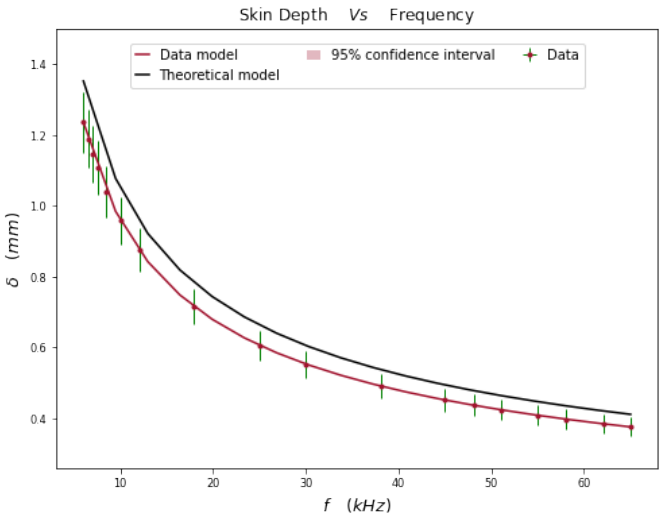

(b) Skin depth plotted against frequency.

Fig. 2: Plots of data obtained using a brass conductor.

Regardless of the vertical offset, both sets of data follow the same exponential shape.

Rod	R' (mm)	σ (MS/m)	δ (mm)
Brass	5.10±0.03	27.5±3.5	0.716±0.061
Aluminium	5.26±0.03	50.8±6.6	0.643±0.042
Copper	5.61±0.04	68.9±9.2	0.553±0.037

Table 2: Mean experimental data determined for each conducting rod. δ is given for a frequency of $(17929 \pm 10)\ Hz$.

4.2 Aluminium & Copper Conductors

The previous section is repeated for both copper and aluminium conductors. The values obtained for R_r, I_{rms} and B_0 are given in Table 1, and are highly consistent with those for the brass conductor.

Using data from Table 3, V/f is plotted against f^{-2} in Fig. 5a and 5c. The model plot functions for aluminium and copper are:

$$\frac{V}{f} = f^{-\frac{1}{2}}(6.91 \pm 0.14)10^{-5} + (4.57 \pm 0.08)10^{-7} \quad (17)$$

and:

$$\frac{V}{f} = f^{-\frac{1}{2}}(6.20 \pm 0.16)10^{-5} + (6.27 \pm 0.09)10^{-7} \quad (18)$$

Both plots have a strong significant ($p < .001$) correlation ($r = .997, .996$) with a moderate coefficient of determination ($r_2 = .78, .76$).

The values calculated for σ and R' are given in Table 2, and δ in Table 3. The experimental σ for copper and aluminium have percent errors of 95.5 % and 23.0%, respectively. The significant disparity between the theoretical and experimental σ for copper does not necessarily indicate inaccuracy.

For example, the discrepancy could be attributed to temperature. As discussed in Section 2.2, σ is negatively proportional to temperature, which may indicate that the experimental temperature is lower than that of Wiederick's investigation. Wiederick did not note the temperature, however, according to TibTech, σ for aluminium at $20°C$ is 36.9 MS/m. This reduces the percent error by half and suggests that the experiment was conducted at a temperature less that $20°C$.

4.3 Comparison

Fig. 2a, 5a and 5c have been superimposed in Fig. 3a. It is apparent that the brass and aluminium plots have a lower y-intercept (α) than the copper plot. This can be accounted for by the fact that α is proportional to both R and R'. As shown in Table 1, the aluminium and brass conductors have greater R and R' values than copper, and therefore lower y-intercepts. The plots are adjusted to the same intercept in the subplot of Fig. 3a

The significant disparity between the slopes of brass and copper can be reasoned by the fact that brass is an alloy consisting of $\sim 66\%$ copper and 33% zinc. Zinc has a lower conductivity than copper and so it follows

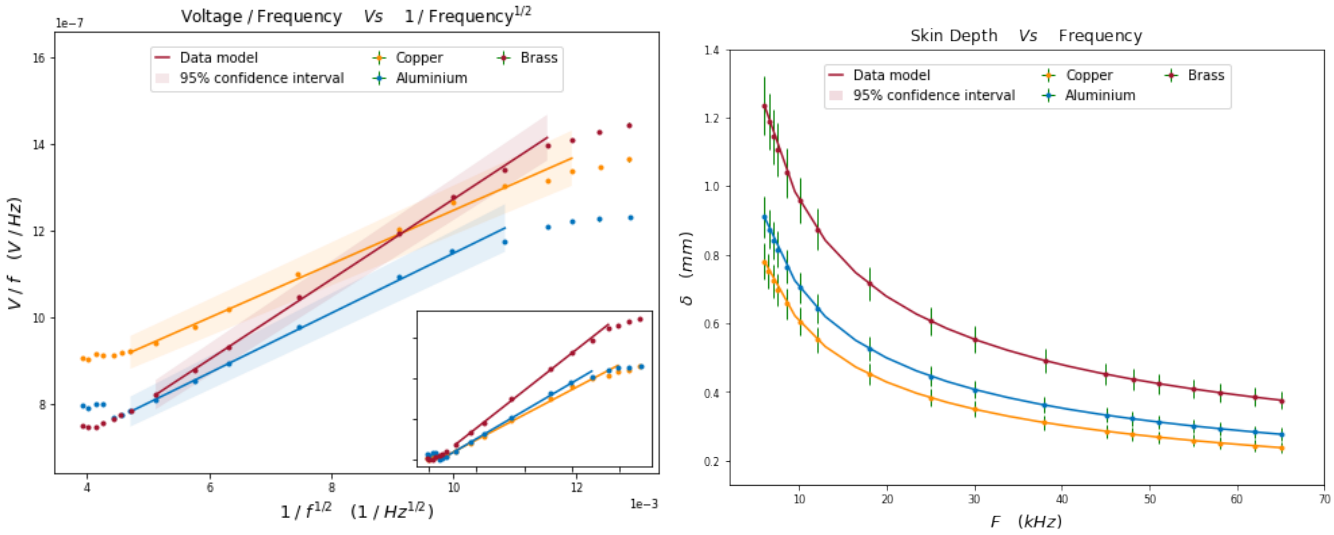

(a) Voltage/frequency plotted against frequency$^{-\frac{1}{2}}$.

(b) Skin depth plotted against frequency.

Fig. 3: Plots of data obtained using aluminium, copper and brass conductors.

that the conductivity of a zinc-copper alloy is lower than that of pure copper, as evidenced in Table 2. In Eq. 12, σ is negatively proportional to β and so a greater slope is anticipated for a less-conductive alloy such as brass.

From the subplot it is apparent that the difference in slope between the aluminium and copper plots is less discernible. This can be attributed to the similar conductivity's of copper and aluminium relative to brass.

Fig. 2a, 5b and 5d are also superimposed in Fig. 3b. According to Eq. 6, δ is negatively proportional to σ. Therefore, Fig. 3b further reiterates the similarity in skin depth and conductivity between brass and copper, as well as the disparity between that of brass and aluminium.

It is apparent from the data that copper has the greatest electrical conductivity, followed by aluminium and brass. Similarly, from a given frequency, copper has the smallest skin depth, followed by aluminium and brass. It can be concluded that skin depth is inevrsely proportional to conductivity.

All model plots in Fig. 5a - 5d coincide fairly well with the shape and position of their corresponding theoretical plots. Therefore, it can be concluded that the experimental findings conform to Eq. 6 and also support the validity of the derivation resulting in Eq. 8 and Eq. 9.

The data models in Fig. 2a, 5a and 5c are based on a mean of 8 out of the total 18 data points. Due to the boundary condition in Eq. 7 and the magnetic saturation of the conductors, the majority of the data recorded is not pertinent to the determination of σ and δ. Ideally, more data points should be recorded within the relevant range to improve experimental accuracy and efficiency.

The metal conductors appear to attain magnetic saturation at approximately the same frequency ($\sim 7518\ Hz$).

5 Conclusion

The phenomenon of skin effect is demonstrated and examined using induced magnetism in brass, aluminium and copper conductors.

Plots of voltage/frequency against $1/\text{frequency}^{1/2}$ for each metal reveal a significant linear positive correlation. From these plot, the mean radius of the inner solenoid, the skin depth and the electrical conductivity of each metal is determined.

Plots of skin depth against frequency reveal a negative exponential correlation within the kHz range. Copper has the greatest skin depth for a given frequency, followed by aluminium and brass.

Their corresponding conductivities are calculated to be (68.9 ± 9.2), (50.8 ± 6.6), and (27.5 ± 3.5) MS/m. The experimental data confirms that skin depth is inversely proportional to electrical conductivity i.e better conductors experience reduced effective area.

Appreciable discrepancies between the theoretical and model plots indicate the instance of magnetic saturation and reduced experimental temperature. Such factors interfere with the capacity for accurate data analysis and should be minimised.

Overall, the experimental findings coincide to a fair degree with both theory and a study undertaken under similar conditions.

References

[1] D. Griffiths, "Electrodynamics," in *Introduction to Electrodynamics*, ch. 7, pp. 292–313, New Jersey: Prentice Hall, 3rd ed., 1991.

[2] E. Hudson, "Inductance & magnetic energy," in *Physics 8.02: Electricity & Magnetism*, ch. 11, pp. 3–10, Massachusetts: Massachusetts Institute of Technology, 2007.

[3] "Magnetic permeability," in *Nondestructive Evaluation Physics : Materials*, Iowa State University. `https://www.nde-ed.org/Physics/Materials/Physical_Chemical/Electrical.xhtml`(visited: 2021-04-02).

[4] P. Ribiero, "Electric and magnetic circuits," in *Standard Handbook for Electrical Engineers*, ch. 2, pp. 2–50, McGraw-Hil, 2006.

[5] H. Wiederick and N. Gauthier, "Frequency dependence of the skin depth in a metal cylinder," *American Journal of Physics*, vol. 51, no. 2, pp. 175–176, 1983. doi: `10.1119/1.13319`.

[6] P. Yang, "Analysis of peak electromagnetic torque characteristics for superconducting dc induction heaters," *IEEE Access*, vol. 8, p. 14783, 2020. doi: `10.1109/ACCESS.2019.2963718`.

6 Appendix

6.1 Theory

In the experiment, the multimeter measures the root mean square of the current. This can be transformed into I_0 where:

$$I_0 = \sqrt{2} I_{rms} \tag{19}$$

7 Selection Method

The range of data to which the data models are fitted is selected so as to avoid regions of magnetic saturation. It is presumed that that the rightmost portion of the data in Fig. 2a levels off due to saturation. This is best visualised in Fig. 4 in which an increase in secondary voltage and therefore frequency, no longer caused a reduction of the skin depth. At this point, the magnetic flux and back-emf are maximised and constant.

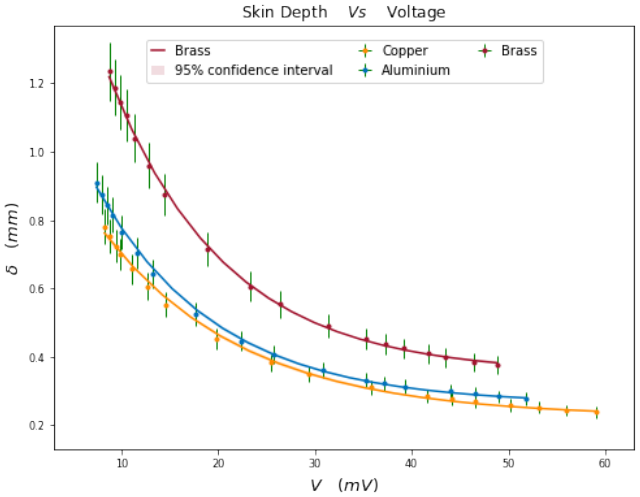

Fig. 4: Skin depth plotted against secondary voltage.

The data range is also selected so as to maximise adherence to Eq. 7 using the values of R and R' from Tables 1 and 2. Total adherence is successfully achieved for the brass model. However, indices 6-17 and 8-17 of the copper and aluminium data fail to meet the boundary condition. For practicality, δ values greater by up to 0.11 mm, and 0.29 mm and are accepted for use within the aluminium and copper data models, respectively.

7.1 Tables & Figures

Rod	f (Hz)	V (mV)	δ (mm)
Brass	6033±10	8.72±0.02	1.187±0.089
	6518±10	9.31±0.02	1.141±0.085
	7027±10	9.91±0.02	1.100±0.082
	7518±10	10.50±0.02	1.063±0.079
	8507±10	11.40±0.02	0.999±0.075
	10012±10	12.80±0.02	0.921±0.069
	12049±10	14.40±0.02	0.840±0.063
	17929±10	18.80±0.02	0.688±0.051
	25022±10	23.30±0.02	0.583±0.044
	30028±10	26.40±0.02	0.532±0.040
	38079±10	31.30±0.02	0.472±0.035
	45030±10	35.30±0.02	0.434±0.032
	48205±10	37.30±0.02	0.420±0.031
	51015±10	39.10±0.02	0.408±0.030
	55035±10	41.70±0.02	0.393±0.029
	58121±10	43.50±0.02	0.382±0.029
	62059±10	46.40±0.02	0.370±0.028
	65033±10	48.80±0.02	0.361±0.027
Copper	6017±10	7.41±0.02	0.845±0.059
	6526±10	8.01±0.02	0.811±0.057
	7007±10	8.57±0.02	0.783±0.055
	7496±10	9.06±0.02	0.757±0.053
	8509±10	10.00±0.02	0.711±0.050
	10052±10	11.60±0.02	0.654±0.046
	12049±10	13.20±0.02	0.597±0.042
	17977±10	17.60±0.02	0.489±0.034
	25081±10	22.40±0.02	0.414±0.029
	30074±10	25.70±0.02	0.378±0.026
	38012±10	30.80±0.02	0.336±0.023
	45080±10	35.30±0.02	0.309±0.022
	48018±10	37.20±0.02	0.299±0.021
	51065±10	39.30±0.02	0.290±0.020
	55003±10	44.00±0.02	0.279±0.019
	58124±10	46.50±0.02	0.272±0.019
	62022±10	49.00±0.02	0.263±0.018
	65078±10	51.80±0.02	0.257±0.018
Aluminium	6035±10	8.24±0.02	0.760±0.051
	6500±10	8.76±0.02	0.732±0.049
	7021±10	9.40±0.02	0.704±0.047
	7513±10	9.89±0.02	0.681±0.046
	8513±10	11.10±0.02	0.640±0.043
	10025±10	12.70±0.02	0.590±0.040
	12035±10	14.50±0.02	0.538±0.036
	18015±10	19.80±0.02	0.440±0.030
	25055±10	25.50±0.02	0.373±0.025
	30008±10	29.40±0.02	0.341±0.023
	38025±10	35.80±0.02	0.303±0.020
	45084±10	41.60±0.02	0.278±0.019
	48043±10	44.20±0.02	0.269±0.018
	51021±10	46.60±0.02	0.261±0.018
	55003±10	50.20±0.02	0.252±0.017
	58104±10	53.20±0.02	0.245±0.016
	62034±10	56.00±0.02	0.237±0.016
	65094±10	59.10±0.02	0.231±0.016

Table 3: Experimental data obtained for each conducting rod.

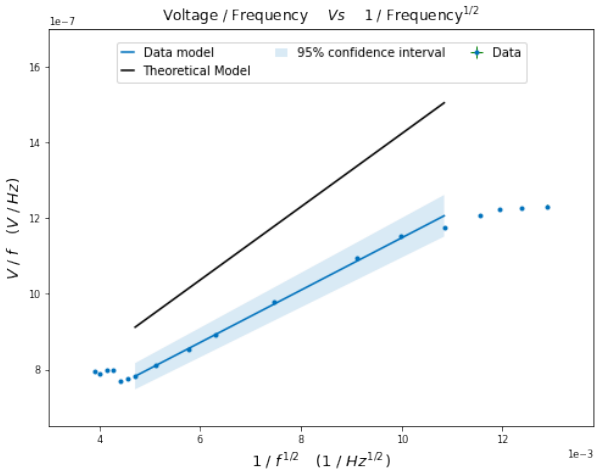

(a) Voltage/frequency plotted against frequency$^{-\frac{1}{2}}$.

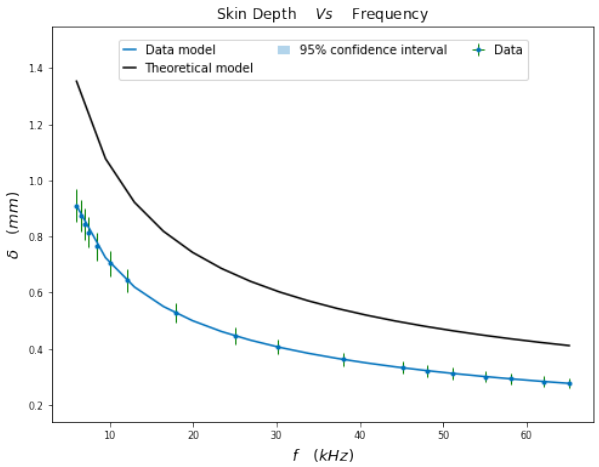

(b) Skin depth plotted against frequency.

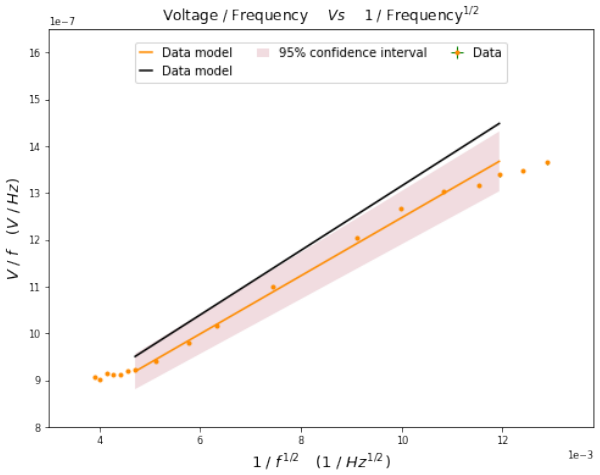

(c) Voltage/frequency plotted against frequency$^{-\frac{1}{2}}$.

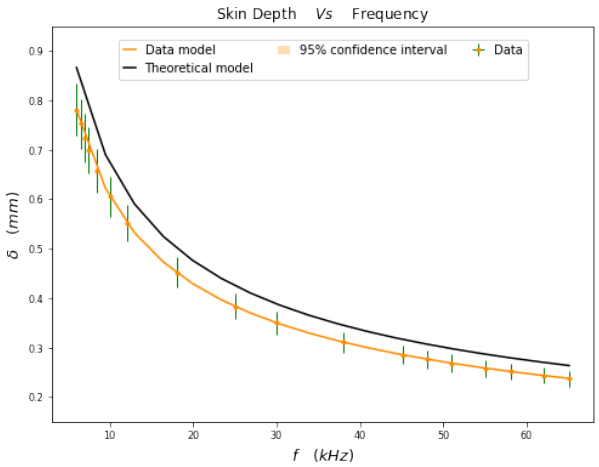

(d) Skin depth plotted against frequency.

Fig. 5: Plots of data obtained using a copper (top row) and aluminium (bottom row) conductor.